frontiers | Frontiers in Earth Science

TYPE Original Research
PUBLISHED 13 December 2023
DOI 10.3389/feart.2023.1323413

OPEN ACCESS

EDITED BY
Mingtao Li,
Linyi University, China

REVIEWED BY
Xin Shan,
Ministry of Natural Resources, China
Zhong Han,
Chengdu University of Technology, China

*CORRESPONDENCE
Adam D. Woods,
awoods@fullerton.edu

RECEIVED 17 October 2023
ACCEPTED 27 November 2023
PUBLISHED 13 December 2023

CITATION
Woods AD, Zonneveld J-P and Wakefield R (2023), Hyperthermal-driven anoxia and reduced productivity in the aftermath of the Permian-Triassic mass extinction: a case study from Western Canada.
Front. Earth Sci. 11:1323413.
doi: 10.3389/feart.2023.1323413

Hyperthermal-driven anoxia and reduced productivity in the aftermath of the Permian-Triassic mass extinction: a case study from Western Canada

Adam D. Woods[1]*, John-Paul Zonneveld[2] and Ryan Wakefield[1]

[1]Department of Geological Sciences, California State University, Fullerton, CA, United States, [2]Department of Earth and Atmospheric Sciences, University of Alberta, Edmonton, AB, Canada

Introduction: The eruption of the Siberian Traps near the Permian-Triassic boundary (PTB) resulted in the rapid input of vast amounts of CO_2 into the atmosphere and the subsequent development of a hothouse climate across much of the Early Triassic. The distribution of environmental stresses led to a complex recovery as survivors navigated high SSTs in shallow settings and an expanded OMZ that impinged upon the continental shelves. The Ursula Creek section of western British Columbia preserves a complete Lower-lowermost Middle Triassic sedimentary record of deep-water facies and provides a means to examine how offshore oceanic conditions varied along the western continental margin of Pangaea across the PTB and the entire Permian-Triassic recovery interval.

Methods: A total of 204 samples were collected from the uppermost Permian Fantasque Formation, the Griesbachian—Dienerian Grayling Formation and the Smithian—Anisian Toad Formation and analyzed for major, minor, and trace elements in addition to %TOC contents.

Results: Anoxic to euxinic conditions were persistent during deposition of most of the study interval based on lithologic indicators (finely-laminated siltstone that lacks trace fossils and a benthic fauna) and elevated Mo, U, and V enrichment factors (EFs). Ba, Cu, Ni, P, and Zn EFs indicate dampened productivity (EFs <1) across the much of the Early Triassic that was the result of weakened upwelling during a global hothouse interval. An increase in Cu, Ni, P, and Zn enrichment factors during the Anisian track a decline in global temperatures and the reestablishment of coastal upwelling as global thermal gradients and wind speeds increased.

Discussion: The results of this study point to the persistence of hyperthermal events and associated environmental stressors and underscores the urgency of curbing modern greenhouse gas emissions to prevent Earth from tipping into a hothouse state.

KEYWORDS

Permian-Triassic mass extinction, anoxia, productivity, upwelling, trace elements

Introduction

The Permian-Triassic mass extinction (PTME) was the most devastating biotic crisis in Earth history (Raup, 1979; Erwin, 1993; Alroy et al., 2008), both on land (Sahney and Benton, 2008) and in the oceans (Stanley, 2016; Fan et al., 2020). The extinction was driven by the eruption of the Siberian Traps (e.g., Renne et al., 1995; Wignall, 2001; Rampino et al., 2017; Green et al., 2022), which input tremendous amounts of CO_2 into the atmosphere (e.g., Kidder and Worsley, 2010; Black et al., 2015; Sobolev et al., 2015; Burgess et al., 2017; Joachimski et al., 2022; Tian and Buck, 2022), leading to a runaway greenhouse effect that made life in shallow tropical seas untenable for many organisms (Sun et al., 2012; Romano et al., 2013; Song et al., 2014). Global hothouse conditions led to sluggish oceanic circulation (Kidder and Worsley, 2004; Kiehl and Shields, 2005; Kiehl and Shields, 2010) and the depletion of oxygen in the deep ocean (Isozaki, 1997; Grasby et al., 2013; Grasby et al., 2021; Takahashi et al., 2021), as well as the impingement of anoxic water masses onto the continental shelves (e.g., Wignall and Hallam, 1992; Thomas et al., 2004; Algeo et al., 2007; Galfetti et al., 2008; Grasby and Beauchamp, 2009; Liao et al., 2010; Metcalfe et al., 2013; Pietsch et al., 2014; Lau et al., 2016; Xiao et al., 2018). Consequently, marine life was in a precarious position: squeezed from above by hot sea surface temperatures and from below by a shallow redoxocline, resulting in a narrow habitable zone whose dimensions varied as global temperatures warmed or cooled, and the redoxocline rose and fell (Beatty et al., 2008; Song et al., 2014; Woods et al., 2019). Geochemical records and geochronology indicate that the Early Triassic global hothouse persisted until the end of the Early Triassic (Sun et al., 2012; Joachimski et al., 2022), while anoxia in the deep ocean may have persisted into the mid-Anisian (lower Middle Triassic) (Isozaki, 1997; Lau et al., 2016; Ishizaki and Shiino, 2023).

Palaeoenvironmental reconstructions of the Permian-Triassic interval have primarily focused on the period of time surrounding the PTME (e.g., Wignall and Twitchett, 1996; Lehrmann et al., 2003; Thomas et al., 2004; Algeo et al., 2007; Son et al., 2007; Grasby and Beauchamp, 2009; Bond and Wignall, 2010; Brookfield et al., 2010; Liao et al., 2010; Richoz et al., 2010; Varol et al., 2011). Only a handful of studies have produced continuous environmental records across the entire Lower Triassic interval of environmental instability at the regional or local scale (e.g., Shen et al., 2015; Lau et al., 2016; Grasby et al., 2021; Ishizaki and Shiino, 2023; Saito et al., 2023). Analysis of paleobiologic trends during this period suggests that recovery was often sluggish or reset by persistent environmental stresses (Pietsch et al., 2014; Song et al., 2014; Woods et al., 2019), resulting in a slow biotic rebound that frequently stretched well beyond the earliest Triassic, to perhaps as late as the early middle Triassic (Anisian) (e.g., Schubert, 1989; Hallam, 1991; Twitchett and Wignall, 1996; Boyer et al., 2004; Pruss and Bottjer, 2004; Twitchett and Barras, 2004; Nützel and Schulbert, 2005; Baucon and De Carvalho, 2016; Golding, 2021; Wang et al., 2022; Zhu et al., 2022). It is important, therefore, to produce longer palaeoenvironmental records that allow us to better understand the complex relationship between biotic trends and environmental conditions, and, as a result, how the planet and its biota recover from protracted, multifaceted environmental crises, including the hyperthermal event associated with the PTME or our modern climate emergency.

Sedimentary sequences from the Western Canada Sedimentary Basin (WCSB) provide a means to reconstruct continuous palaeoenvironmental records across the entire Permian-Triassic hyperthermal event and study the effects of an extreme global hothouse on palaeoceanographic conditions along the eastern edge of the Panthalassic superocean. The Ursula Creek, British Columbia, Canada locality contains a continuous record of sedimentation in a deep water setting from the Permian through the later Middle Triassic (Henderson, 1997; Wignall and Newton, 2003; Zonneveld et al., 2010a; Playter et al., 2017; Henderson et al., 2018; Zonneveld and Moslow, 2018). Prior palaeoceanographic studies have focused primarily on the PTB interval (e.g., Wang et al., 1994; Wignall and Twitchett, 1996; Wignall and Newton, 2003; Brookfield et al., 2022); the aim of the current study is to create a record of deep-water (below apparent storm water wave base; Zonneveld, 2010) palaeoenvironmental conditions across the entire post-extinction recovery interval in order to gain a better understanding of the effects of hyperthermal events on palaeoceanographic conditions and the relationship between biotic recovery and long-lasting environmental stress.

Geologic setting

The Western Canada Sedimentary Basin (WCSB) was situated along the northwestern margin of Pangaea, centered near 30° N palaeolatitude, and rotated roughly 30° clockwise from its present-day position from the Permian to the Early Triassic (Figure 1A). The WCSB faced west towards the Panthalassic Ocean and was subjected to seasonally-variable coastal upwelling during the Permian (Davies, 1997b). The combination of cold-water coastal upwelling, north to northeasterly trade winds, and a 30° N palaeolatitude led to the development of an arid climate onshore of the WCSB that is similar to what is observed today in the southwestern United States and northwestern Mexico (Davies, 1997b; Beauchamp and Baud, 2002).

The Early Triassic was an interval of active tectonism in the area of the present-day Western Canada Sedimentary Basin (WCSB). Pericratonic terranes, which had separated from North America during expansion of the Slide Mountain Sea during the Paleozoic, were thrust back onto the North American margin during the Early Triassic, reactivating older structural elements and causing increased subsidence in the region of the collapsed Peace River Arch (Ferri and Zonneveld, 2008; Rohais et al., 2018; Zonneveld and Moslow, 2018). This area is often referred to as the Peace River Embayment and has been referred to as the Peace River Basin (Davies et al., 1997).

Lower Triassic sedimentary rocks in the Peace River Basin (PRB) were deposited in a wide range of depositional settings including marginal marine, shoreface deltaic, and proximal to distal offshore in a low-relief clastic ramp setting (e.g., Davies et al., 1997; Orchard and Zonneveld, 2009; Zonneveld et al., 2010a; Zonneveld et al., 2010b; Proverbs et al., 2018; Zonneveld and Moslow, 2018). The rocks that comprise the Ursula Creek section (Figure 1B) include the Upper Permian Fantasque Formation, the Lower Triassic Grayling Formation, the Lower-Middle Triassic Toad Formation, and the Upper Triassic (Carnian) Ludington Formation (Figure 1C) (Zonneveld, 2010). Conodont biostratigraphy suggests that the

10.3389/feart.2023.1323413

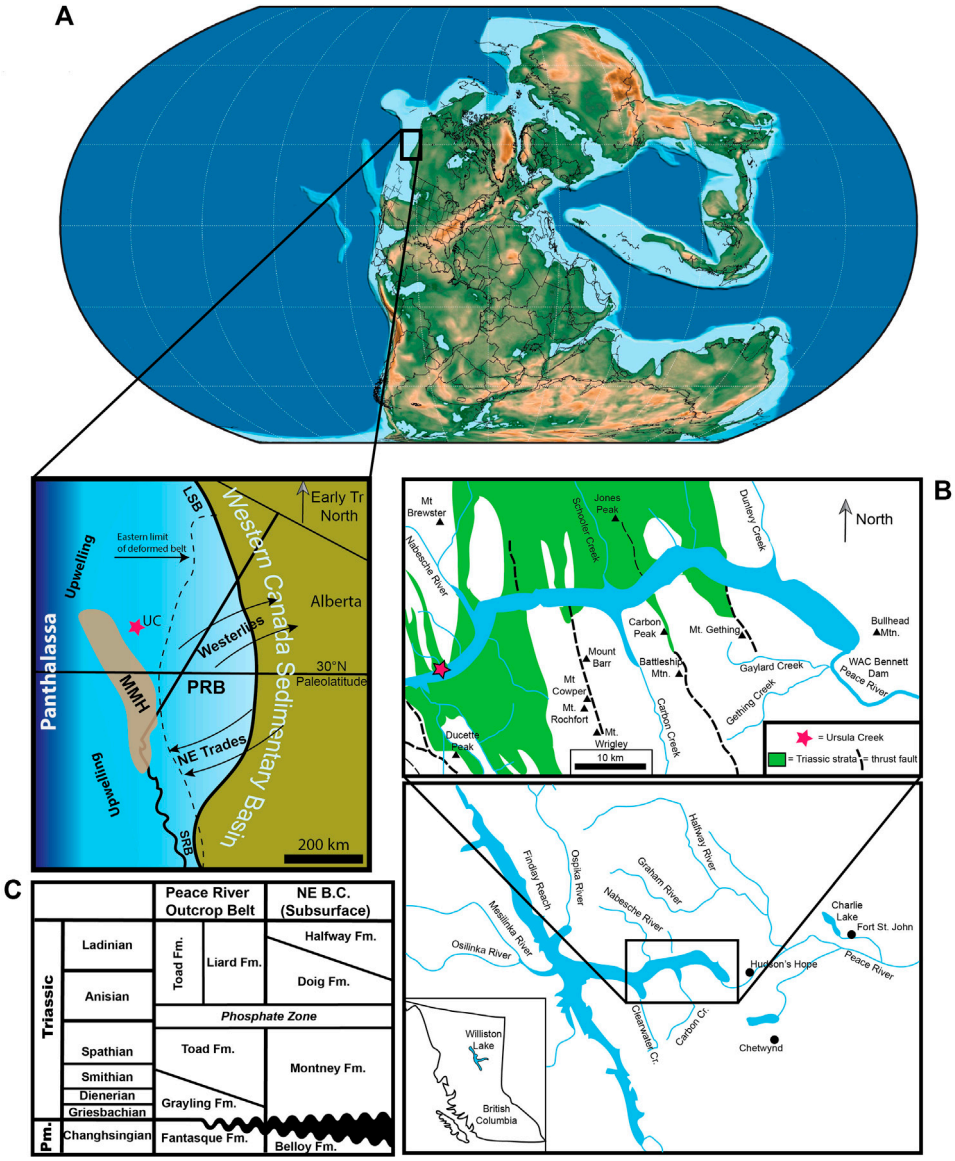

FIGURE 1
Locality map and chronostratigraphy of the WCSB. **(A)** Global and regional palaeogeography of the Western Canada Sedimentary Basin (WCSB) at the Permian-Triassic boundary, approximately 252 Ma. Note that the WCSB straddled 30°N palaeolatitude and was rotated 30° clockwise from today. UC, Ursula Creek; PRB, Peace River Basin; SRB, Spray River Basin; LSB, Liard Sub-basin; MMH, Meosin-Muinok High; Tr, Triassic. Global palaeogeographic map modified from Scotese (2021); regional palaeogeographic information from Playter et al. (2017), Zonneveld and Moslow (2018), and Davies (1997a). **(B)** Williston Lake area, including Triassic outcrop belt and the location of the Ursula Creek study locality. Modified from Zonneveld (2010). **(C)** Chronostratigraphy of northeastern British Columbia. Pm., Permian; Fm., Formation. Modified from Zonneveld (2010) and Tozer (1994).

Permian through lowermost Middle Triassic interval (Changhsingian through Anisian) records continuous deposition, whereas the later Middle Triassic and Upper Triassic intervals are separated by an erosional unconformity that removed most of the Ladinian section (Henderson, 1997; Wignall and Newton, 2003; Zonneveld et al., 2010a; Playter et al., 2017; Henderson et al., 2018; Zonneveld and Moslow, 2018).

The uppermost Permian (upper Changhsingian; Henderson and Mei, 2000) Fantasque Formation is made up of radiolarian and spiculitic chert (Wignall and Newton, 2003; Brookfield et al., 2022) with thin shale interbeds (Wignall and Newton, 2003) that increase in frequency towards the top of the section. Much of the Fantasque Formation was deposited under oxygenated conditions based on the presence of macroburrows in the lower part of the formation, including *Conichnus*, *Diplocraterion*, *Planolites*, *Rosselia*, and *Teichichnus*, but a shift to microburrowed chert, Th/U values that drop below 3, and the presence of discrete, laminated siltstone and shale horizons in the upper portion of the unit indicates the establishment of oxygen-limited conditions (Wignall, 1994; Wignall and Twitchett, 1996; 2002; Wignall and Newton, 2003; Playter et al., 2017).

The contact between the Fantasque Formation and overlying Grayling Formation is conformable and sharp, with tan chert

replaced by black bituminous siltstone and tan dolomitic siltstone (Wignall and Newton, 2003; Zonneveld et al., 2010a; Playter et al., 2017). Previous work on the Ursula Creek section placed the PTME at the lithologic contact between the Fantasque and Grayling Formations and the PTB approximately 80 cm above the lower contact of the Grayling Formation based on the first appearance of the conodont *Hindeodus parvus* (Wignall and Newton, 2003). A lack of macrofauna and bioturbating organisms led Wignall and Newton (2003) to conclude that deposition of the Grayling Formation at Ursula Creek occurred under anoxic conditions, while previously-published geochemical data reveals the establishment of anoxic conditions across the Permian-Triassic boundary (PTB) and Griesbachian based on analysis of Th/U ratios (Wignall and Newton, 2003), platinum group elements (Brookfield et al., 2010; Brookfield et al., 2022), and trace elements (Brookfield et al., 2022).

The Toad Formation at Ursula Creek consists of black siltstone that is interbedded with carbonate and coarse siltstone/very fine-grained sandstone in the lower portion of the section (lower 34.5 m), and black siltstone that contains abundant phosphate nodules higher in the section (next 19.9 m). The uppermost 30.9 m of the Toad Formation at Ursula Creek is Ladinian in age (Gibson and Edwards, 1992; Orchard and Tozer, 1997), and was not examined for this study. Brookfield et al. (2022) assign a Spathian age to the Toad Formation in Figure 3 of their paper, while they ascribe a mid-Dienerian age to the base of the unit (page 901). We follow the interpretation of Orchard and Tozer (1997) who assign an early Smithian age to the base of the Toad Formation at Ursula Creek based on the presence of the conodont *Neogondolella mosheripakistanensis* (=*Neospathodus pakistanensis*) (Gibson and Edwards, 1990; Orchard and Tozer, 1997). Trace element data (Mo/U, Th/U, and Ni/Co) from Brookfield et al. (2022) indicates that the lower ~10 m of the Toad Formation was deposited under dysoxic conditions, while Wignall and Newton (2003) suggest that the laminated, unfossiliferous nature of the unit is indicative of deposition under anoxic conditions. The few fossils that have been previously collected from the Toad Formation comprise actinopterygian fish and ammonoid impressions (Wignall and Twitchett, 2002), which occupied the upper part of the water column, within the habitable zone.

Siliciclastic sediment in the Lower Triassic succession in the WCSB is dominated by fine to medium silt-sized fractions (μm) with subordinate very fine to fine sandstone, and contains an anomalously low proportion of clay, even in distal offshore successions (Zonneveld and Moslow, 2018). This is interpreted to be a function of prolonged, severe aridity in the sediment source area and sediment delivery to the basin dominated by ephemeral fluvial and deltaic systems augmented by aeolian reworking and transport (Zonneveld and Moslow, 2014; Zonneveld and Moslow, 2018). The only true shale in the basin occurs in delta front and prodeltaic successions deposited by sparsely-distributed perennial river deltas (Zonneveld and Moslow, 2014; Zonneveld and Moslow, 2018).

Well to the south, outside of the PRB but within the greater WCSB, Schoepfer et al. (2013) examined palaeoenvironmental changes using sedimentary rocks exposed at the Opal Creek, Alberta, Canada locality. Based on palaeoceanographic modeling and geochemical analyses of samples ranging from ~10 m below the extinction to ~25 m above the event horizon, Schoepfer et al. (2013) confirmed the presence of a Late Permian high-productivity shelf driven by cold-water upwelling that dissipated near the PTB (Beauchamp and Baud, 2002; Schoepfer et al., 2013). Anoxic conditions briefly intensified across the PTME, which Schoepfer et al. (2013) attribute to increased terrestrial weathering rates and nutrient delivery immediately following the extinction (Sephton et al., 2005; Algeo and Twitchett, 2010; Algeo et al., 2011). Extreme global warming during the earliest Triassic led to the cessation of coastal upwelling, constrained the movement of bottom waters, and restricted nutrient input to terrestrial sources, dampening regional productivity and limiting benthic oxygenation (Wang et al., 1994; Wignall and Twitchett, 2002; Schoepfer et al., 2013).

Methods

The Permian-Triassic extinction and recovery interval were examined at the Ursula Creek locality in north-central British Columbia. Samples were collected from the uppermost Permian Fantasque Formation (3 samples were collected from the uppermost 3 black siltstone interbeds, 0.7, 0.6, and 0.2 m below the contact between the Fantasque Formation and Grayling Formation), the Lower Triassic Grayling Formation and the Lower-Middle Triassic Toad Formation (samples collected every 10 cm in the lower 3 m of the Grayling Formation for a total of 30 samples; every 25 cm from 3.0 to 5.0 m above the base of the Grayling Formation for a total of 8 samples; and every 50 cm across the remainder of the study interval for a total of 163 samples). Overall, 204 samples were analyzed for this study. Samples were powdered and prepared for analysis using the microwave digestion method detailed in Ziegler and Murray (2007). Aqueous samples were analyzed using a Perkin-Elmer 7300DV ICP-OES housed in the Department of Geological Sciences at California State University, Fullerton. Accuracy of results are better than 5% and were determined by measuring duplicate samples every 10th analysis as well as running the SCo-1 standard as an unknown multiple times. Organic carbon contents were measured via the loss on ignition method of Dean (1974).

Palaeoproductivity and palaeoxygenation were determined using an approach that employs the measurement of multiple trace element concentrations, specifically: 1) Ba, Cu, Ni, P, and Zn for determination of palaeoproductivity (Tribovillard et al., 2006); and 2) Mo, U, and V for palaeoxygenation (Tribovillard et al., 2006), coupled with outcrop indicators of palaeoxygenation, including trace fossil type and abundance and macrofossil content (e.g., Savrda, et al., 1984). Major element data was also collected in order to measure changes in lithology.

Trace element data was normalized using Enrichment Factors (EFs), which provide a means to examine if a sample is enriched (EF >1) or depleted (EF <1) relative to average shale values (Wedepohl, 1971; Wedepohl, 1991), while correcting for dilution by varying amounts of mineral phases, including those of biogenic origin (Tribovillard et al., 2006). Enrichment factors are calculated as follows:

$$EF_{Element\ X} = (X/Al)_{Sample} / (X/Al)_{Average\ Shale}$$

Van der Weijden (2002) notes that normalization of trace element data may produce false conclusions, especially when relying on absolute values. Therefore, stratigraphic trends in enrichment factors are given weight over specific values, as suggested by Riquier et al. (2005) and Tribovillard et al. (2006).

10.3389/feart.2023.1323413

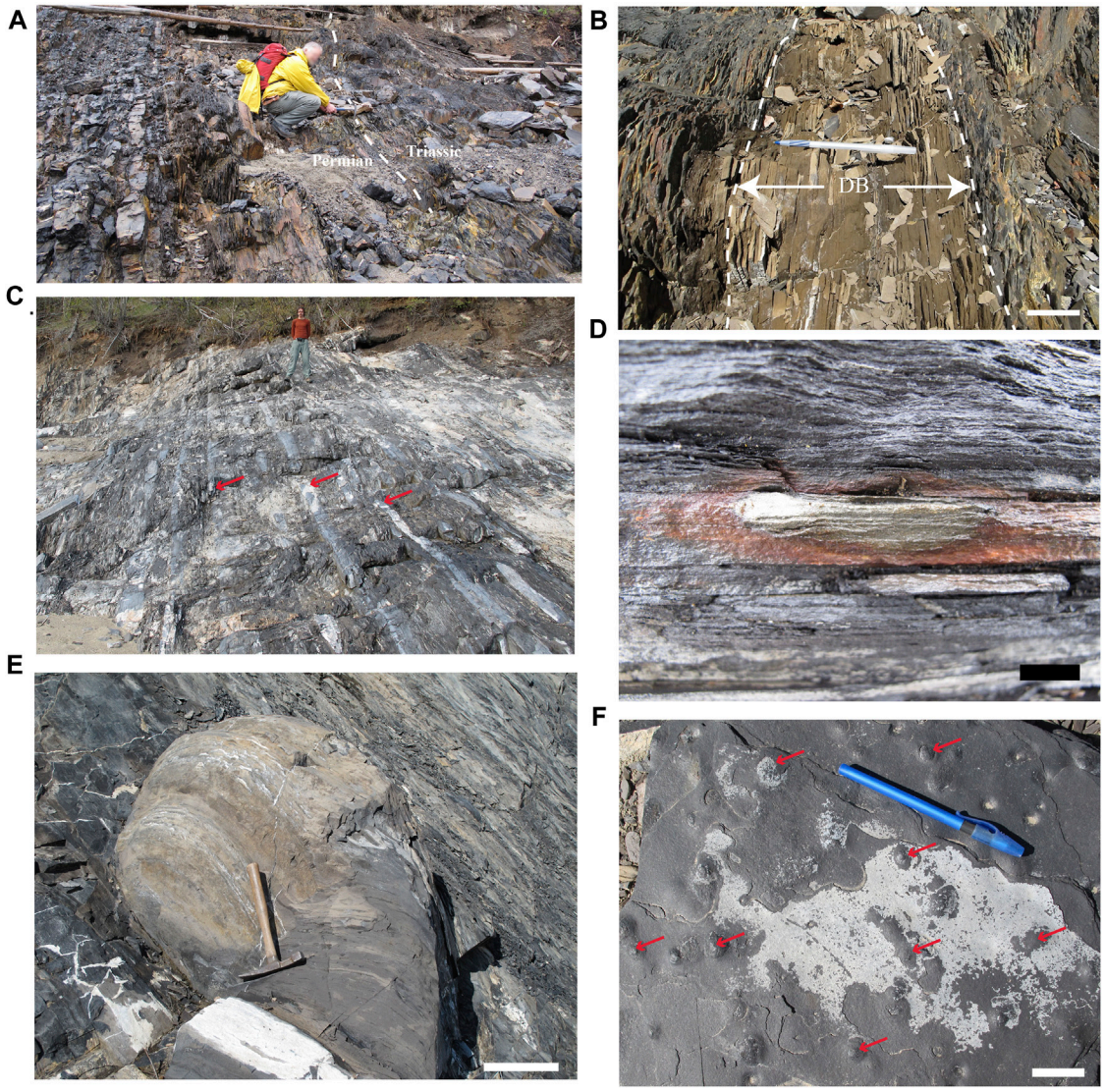

FIGURE 2
Outcrop photos of the study section. **(A)** Permian-Triassic boundary at Ursula Creek. PTB is approximately 80 cm above the contact between the Upper Permian Fantasque Formation, which consists of radiolarian and spiculitic chert with thin shale interbeds, and the black siltstone of the Lower Triassic Grayling Formation. **(B)** The Grayling Formation also contains laminated, tan dolosiltstone beds in the lower 10 m of the unit. DB, dolosiltstone bed. Scale bar = 10 cm. **(C)** The Toad Formation is comprised of black siltstone that is frequently interbedded with turbidites (red arrows). **(D)** Turbidites within the Toad Formation are often associated with detrital pyrite lenses. Scale bar = 1 cm. **(E)** The Anisian portion of the Toad Formation contains large limestone concretions near the base (scale bar = 20 cm), and **(F)** phosphate nodules (red arrows) throughout (scale bar = 5 cm); bedding plane photo.

Results

Lithologic observations

Field observations reveal distinct facies change between the chert of the Upper Permian Fantasque Formation and the overlying fine-grained black siltstone of the Lower Triassic Grayling Formation (Figure 2A). The Grayling Formation is laminated at the mm-scale and contains no trace fossils or evidence of bioturbation (ichnofabric index = 1; Droser and Bottjer, 1986) and lacks benthic fossils. The lower 10 m of the Grayling Formation (20.3–30.3 m) consists of interbedded dark gray laminated bituminous and dolomitic siltstone interbeds that weather a distinct orange-brown color (Figure 2B) (Wignall and Newton, 2003). The overlying Toad Formation is sparsely fossiliferous, consisting of laminated black siltstone throughout, with thin, graded carbonate interbeds (Figure 2C) in the lower 9.6 m (55.6–65.2 m) that consist primarily of broken pelagic bivalve debris, and are interpreted to be turbiditic in origin, and a second turbiditic interval from 79.2–90.1 m consisting of Bouma C-D-E and B-D-E sequences (Zonneveld, 2010). Detrital pyrite is found in layers and lenses associated with many turbidite beds (Figure 2D). The upper 19.9 m of the Toad Formation examined for this study (90.1–110.0 m) consists of black siltstone with large limestone concretions near the base (Figure 2E) and phosphate nodules throughout (Figure 2F). In addition, there is a bedding plane on a limestone bed near the

10.3389/feart.2023.1323413

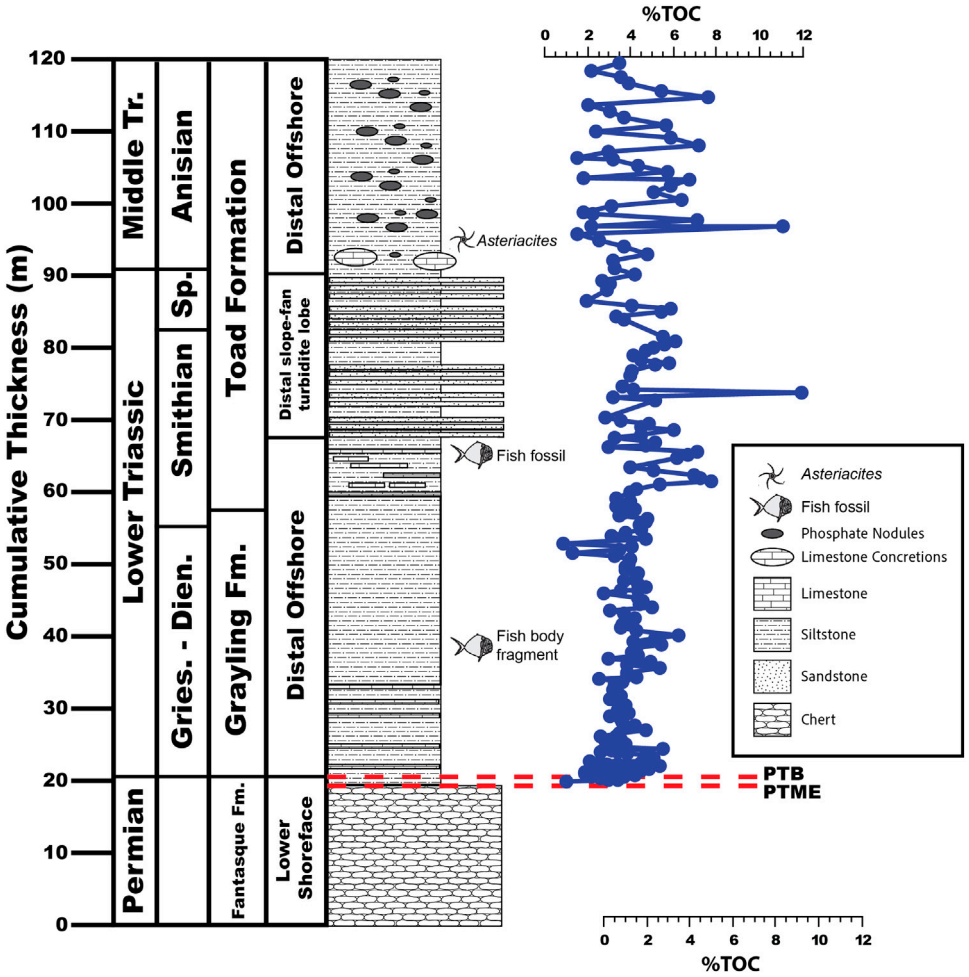

FIGURE 3
Total organic carbon content of the uppermost Fantasque Formation, Grayling Formation, and Smithian-Anisian portion of the Toad Formation, Ursula Creek, BC Canada locality.

base of the phosphatic interval that exhibits a dense, monotypic assemblage of *Asteriacites* trace fossils.

Total organic carbon and major elements

Total organic carbon (TOC) contents range from 0.88%–11.94% (Figure 3), with an overall average value of 4.07% ± 1.46% across the entire section. The Grayling Formation contains less TOC on average (3.71% ± 0.95%) than the Toad Formation (4.48% ± 1.81%). Overall, TOC values undergo an increase across the lower 3.25 m of the Grayling Formation from about 1.03% at the base of the section to 5.04% at 23.55 m. Values remain steady across the remainder of the Grayling Formation (3.83% ± 0.86%) and are higher with greater variability in the Toad Formation (4.48% ± 1.81%).

Major element concentrations appear in Figure 4. SiO_2 is the primary component of both the Grayling Formation (average = 62.82 ± 16.16%) and Toad Formation (average = 54.39 ± 17.84%), while average Al_2O_3 concentrations are 9.24% ± 3.03% for the Grayling Formation and 8.56% ± 3.44% for the Toad Formation. Major element concentrations confirm the presence of dolomite beds in the lower 10 m of the Grayling Formation (Wignall and Newton, 2003), which appears as spikes in %CaO and %MgO that are coupled with drops in $\%SiO_2$ and $\%Al_2O_3$. Otherwise, $\%SiO_2$ and $\%Al_2O_3$ undergo a slight decreasing trend in the upper 15 m of the Grayling Formation (41.3–56.3 m) while %CaO and %MgO exhibit a concomitant increase. Major element concentrations indicate that the upper 35.0 m of the Toad Formation (75.0–110.0 m) examined for this study is more calcareous (greater percentages of CaO and MgO) and contains less detrital matter (lower percentages of SiO_2 and Al_2O_3) than the lower portion of the formation. Otherwise, MnO contents average 0.03% ± 0.05% across the entire study interval.

Palaeoxygenation and palaeoproductivity

Molybdenum, U, and V EFs average 18.89 ± 13.42, 9.79 ± 48.93, and 2.87 ± 4.04, respectively, across the uppermost Fantasque and

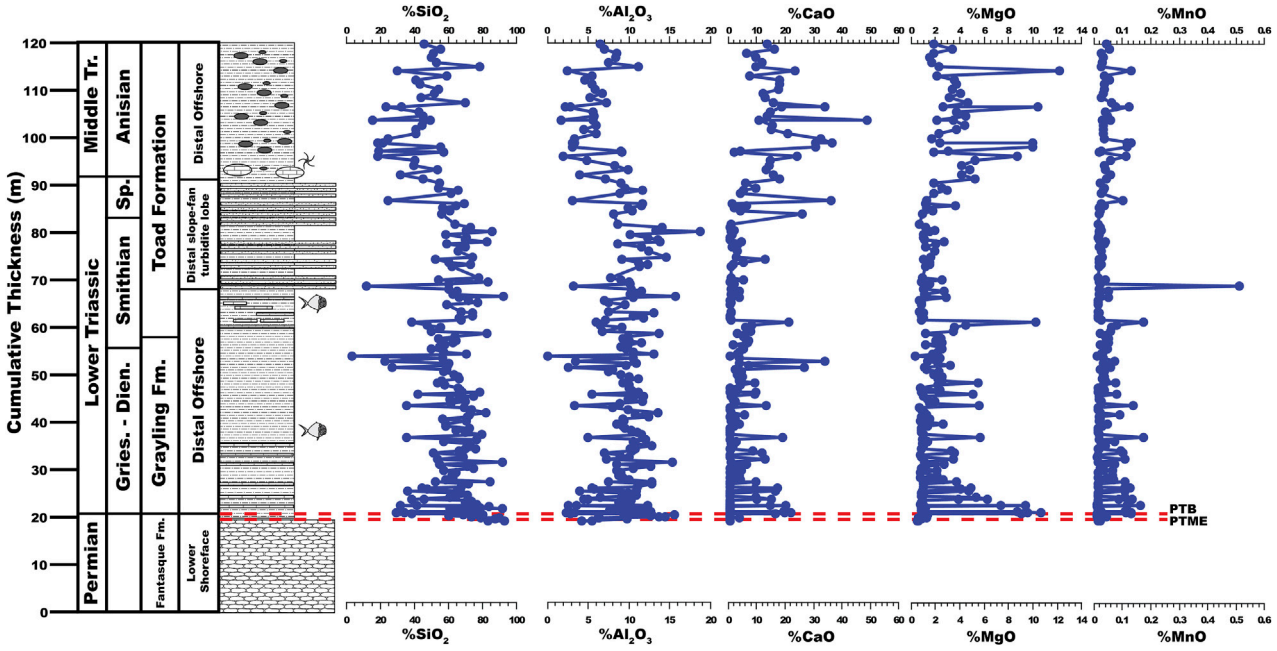

FIGURE 4
Major element composition of the uppermost Fantasque Formation, Grayling Formation, and Smithian-Anisian portion of the Toad Formation, Ursula Creek, BC Canada locality.

Grayling Formations, and 33.03 ± 36.19, 8.12 ± 24.96, and 8.27 ± 9.99, respectively, across the Toad Formation (Figure 5). With regards to the PTB interval (Figure 6), Mo, U, and V EFs each undergo an increase across the PTME, with Mo EFs rising from 0.13 at 20.1 m to 23.72 at 20.5 m, U EFs increasing from 0.58 at 20.1 m to 14.87 at 20.7 m and V EFs rising from 1.15 at 20.1 m to 4.60 at 20.4 m. Enrichment factors decline to lower values just above the PTB at 20.9 m (5.14, 0.42 and 1.55 for Mo, U, and V, respectively). Three distinct trends in palaeoxygenation proxies following the PTB interval are noted: 1) lower Grayling Formation (20.9–40.3 m), where values stay relatively stable (Mo EFs = 14.97 ± 7.52; U EFs = 4.16 ± 8.82; V EFs = 1.87 ± 0.51); 2) upper Grayling Formation and turbiditic portion of the Toad Formation (40.3–90.3 m), where values are higher, and exhibit a greater degree of variability (Mo EFs = 28.91 ± 23.48; U EFs = 12.75 ± 57.60; V EFs = 4.77 ± 5.14); and, 3) phosphate nodule-bearing portion of the Toad Formation (93.3–120 m), where Mo and V EFs undergo a steady increase from 3.33 to 96.37, and 2.02 to 36.37, respectively, while U EFs are typically around 1-2, but exhibit multiple spikes across the interval, ranging from 21.27 (113.8 m) to 118.2 (100.8 m).

Barium, Cu, Ni, P, and Zn EFs average 1.50 ± 1.59, 1.32 ± 1.03, 1.04 ± 1.62, 1.45 ± 1.21, and 0.94 ± 1.80, respectively, across the upper Fantasque and Grayling Formations and 1.44 ± 0.82, 2.48 ± 0.93, 2.18 ± 5.10, 10.42 ± 32.91, and 5.90 ± 15.73, respectively, across the Toad Formation (Figure 7). With the exception of Ba, all productivity-related trace elements undergo a slow, steady increase across the Grayling Formation and Toad Formation (Figure 7), which is evident in the higher average values in the Toad Formation when compared to the upper Fantasque and Grayling Formations. With regards to the PTB interval, Ba, Cu, Ni, and P EFs all increase slightly across the PTME, from 1.14 to 2.17, 1.55 to 2.10, 0.52 to 1.50, and 1.20 to 1.95, respectively, while Zn EFs increase just above the boundary from 0.02 to 7.17. Cu, Ni, and P EFs undergo a steady decline from just above the PTME and across PTB (Figure 8), with Cu declining from 2.10 to 0.27 at 21.1 m, Ni decreasing from 1.50 to 0.33 at 21.1 m, and P dropping from 1.95 to 0.21 at 20.9 m. Barium and Zn EFs increase over the same interval, from 2.17 to 16.80 at 20.6 m for Ba and from 0.01 to 2.20 at 20.9 m for Zn. The lower 6 m of the study section (19.6–25.8 m) reveals baseline Ba, Cu, Ni, P, and Zn EFs that are typically <1, but exhibit order of magnitude fluctuations (Figure 8). Nickel, P, and Zn EFs undergo steady increases across the remainder of the study section (from 0.85–3.78, 1.21–3.12, and 0.07–21.82, respectively), while Cu EFs increase from 1.32 to 4.52 at 108.9 m, before decreasing to 2.05 at the top of the study section (Figure 8). Otherwise, Ba EFs are consistent across the uppermost Fantasque and Grayling Formations (average = 1.50 ± 1.59) and Toad Formation (average = 1.44 ± 0.82).

Discussion

Palaeoxygenation

Previous studies of the Ursula Creek section have documented the deterioration of benthic oxygenation across the upper Fantasque Formation based on a decrease in burrow size, Th/U values <3, and the presence of laminated siltstone interbeds (Wignall and Twitchett, 2002; Wignall and Newton, 2003; Playter et al., 2017). A drop in average pyrite framboid diameter across the PTME horizon from 8.5 ± 2.9 μm to 5.8 ± 2.3 μm is interpreted to be

10.3389/feart.2023.1323413

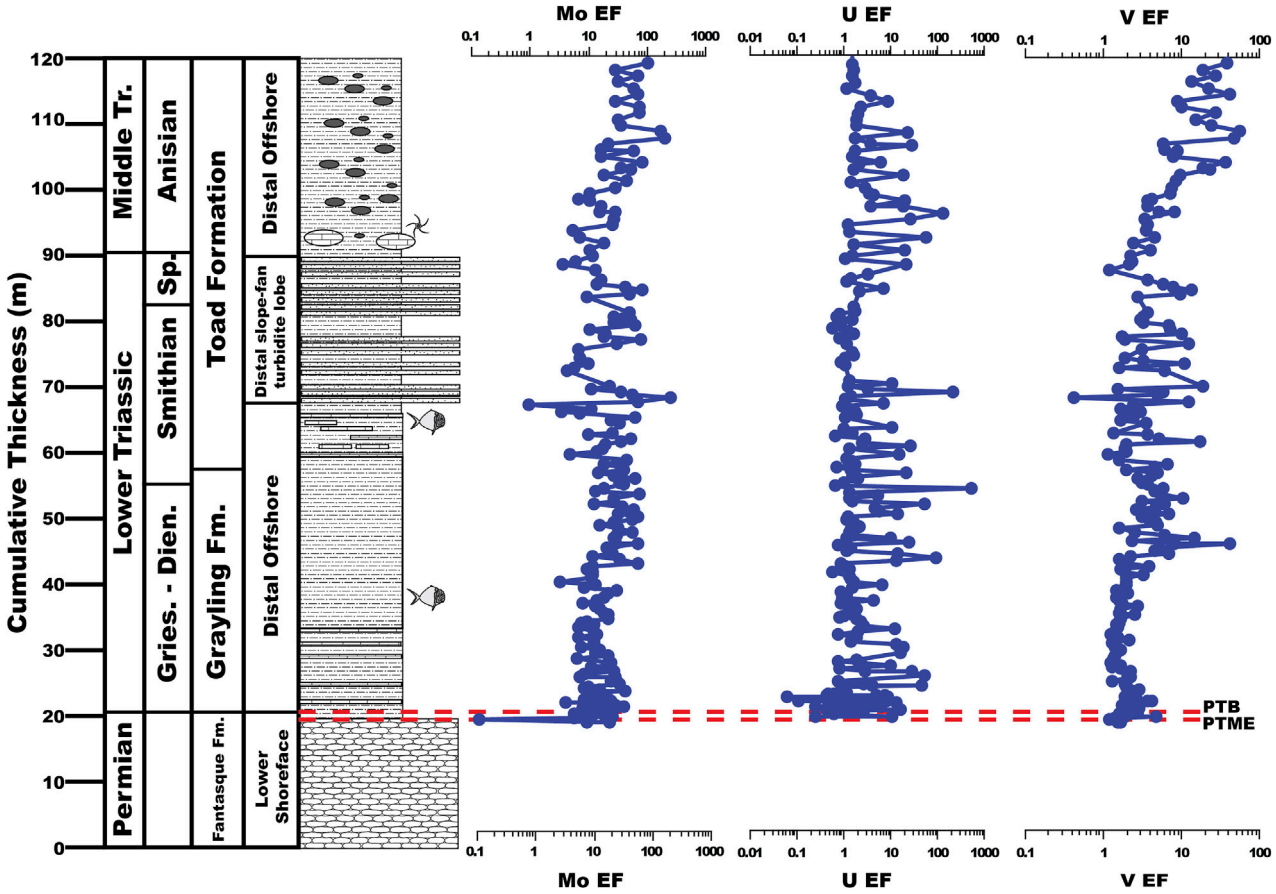

FIGURE 5
Molybdenum, U, and V enrichment factors (EFs) of the uppermost Fantasque Formation, Grayling Formation, and Smithian-Anisian portion of the Toad Formation, Ursula Creek, BC Canada locality.

due to the establishment of euxinic conditions (Wignall and Newton, 2003), while Th/U values across the upper Fantasque, Grayling, and lower 12 m of the Toad Formation are indicative of anoxia (Wignall and Twitchett, 2002). Brookfield et al. (2022) recently examined the same interval using U/Mo, which indicates dysoxic conditions above the PTB, while Ni/Co values suggest dysoxic to anoxic conditions around the PTB and oxygenated conditions above. Relatively low U, V, and Mo concentrations have been documented from other PTB sections (Xiang et al., 2020; Takahashi et al., 2021) and are proposed to be the result of precipitation and removal of redox-sensitive trace metals at abyssal depths within an oxygen-depleted ocean (Algeo, 2004; Xiang et al., 2020; Takahashi et al., 2021). This phenomenon is likely responsible for the contradictory results from previous trace element studies (Wignall and Twitchett, 2002; Playter et al., 2017; Brookfield et al., 2022), and may also be the cause of lower Mo and V EFs in the upper Fantasque and Grayling Formations (18.9 ± 13.4, and 2.9 ± 4.0, respectively) when compared to the Toad Formation (33.0 ± 36.2, and 8.3 ± 10.0, respectively), as well as low U EFs overall (9.0 ± 39.5). As Wignall and Newton (2003) note, the laminated and sparsely fossiliferous nature of the Grayling and Toad Formations provides unambiguous evidence of bottom water anoxia during deposition of both units, while Mo, U, and V EFs are used in the current study to deduce general trends in palaeoxygenation. Mo, U, and V EFs point to a drop in palaeoxygenation across the PTME based on a brief increase in values, followed by a dip in Mo, U and V EFs near the PTB, indicating an improvement in bottom water oxygenation, perhaps from euxinic to anoxic conditions (Figure 6). The steady increase in Mo and V EFs across the Grayling and Toad Formations indicates persistent anoxia that strengthened over time (Figure 5), while higher overall Mo and V values in the Anisian portion of the Toad Formation reflects productivity-driven anoxia (see below). U values do not appear to show an increasing or decreasing trend across the study section, but are typically enriched, and provide another indicator of persistent anoxia.

Palaeoproductivity

Previous studies of productivity across the PTME at Ursula Creek produced mixed results, with Se/Al and Se/TOC (Brookfield et al., 2022) and $\delta^{13}C_{org}$ values (Wang et al., 1994) indicating a productivity drop, while Ba_{bio} signals a slight increase (Brookfield et al., 2022). The current study indicates that productivity increased across the PTME, as reflected by Ba, Cu, Ni, P, and Zn EFs (Figure 8). Productivity was dampened overall in the earliest

10.3389/feart.2023.1323413

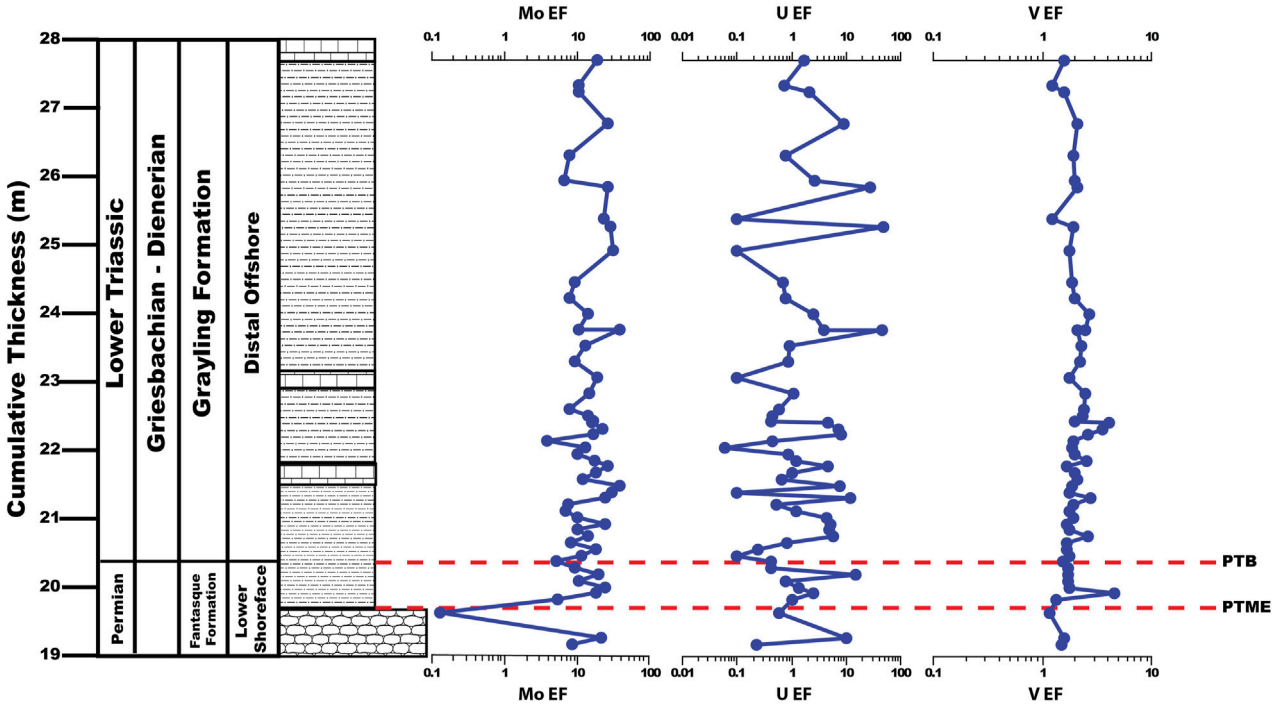

FIGURE 6
Molybdenum, U, and V enrichment factors (EFs) across the PTB interval, Ursula Creek, BC Canada locality.

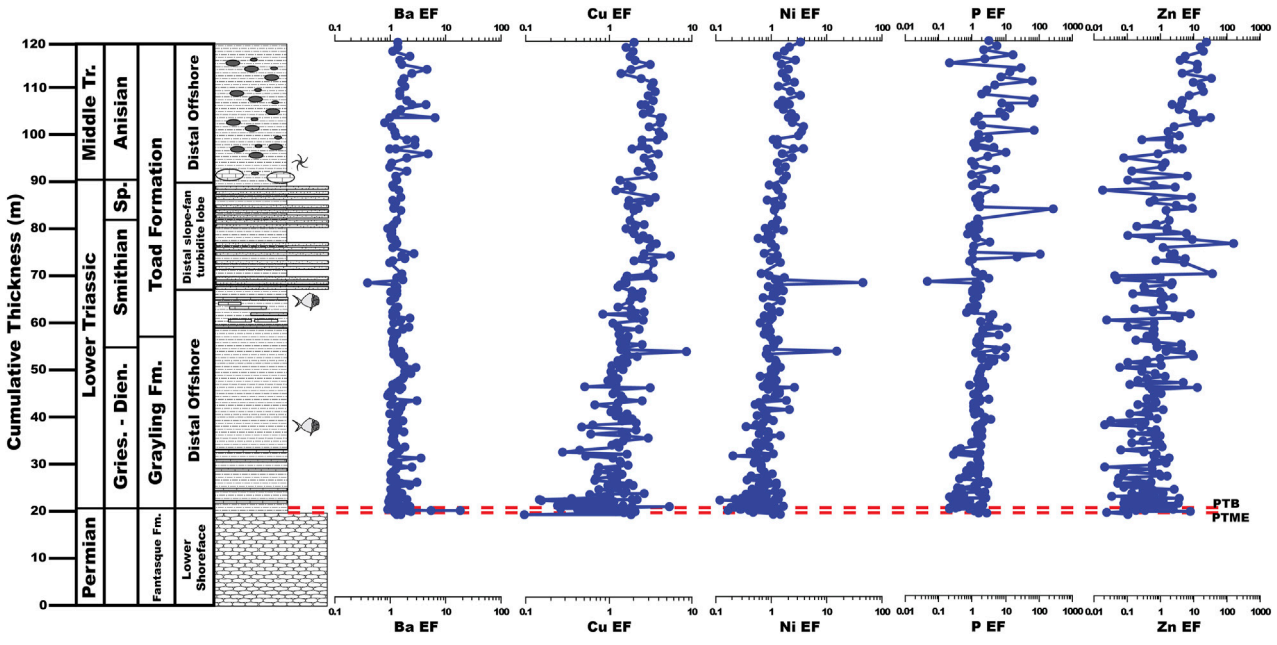

FIGURE 7
Barium, Cu, Ni, P, and Zn enrichment factors (EFs) of the uppermost Fantasque Formation, Grayling Formation, and Smithian-Anisian portion of the Toad Formation, Ursula Creek, BC Canada locality.

Triassic based on Ba, Cu, Ni, P, and Zn EFs that are typically <1 from 19.6–25.6 m, but is followed by a gradual increase in productivity across the remainder of the study section, as reflected by steady increases in Cu, Ni, P, and Zn EFs. This may reflect a shallowing nutricline (Grasby et al., 2016) or a slow increase in productivity over time. Higher P EFs ratios that exhibit large swings of up to 2 orders of magnitude in the Anisian portion of the Toad Formation is expected given the presence of phosphate nodules there.

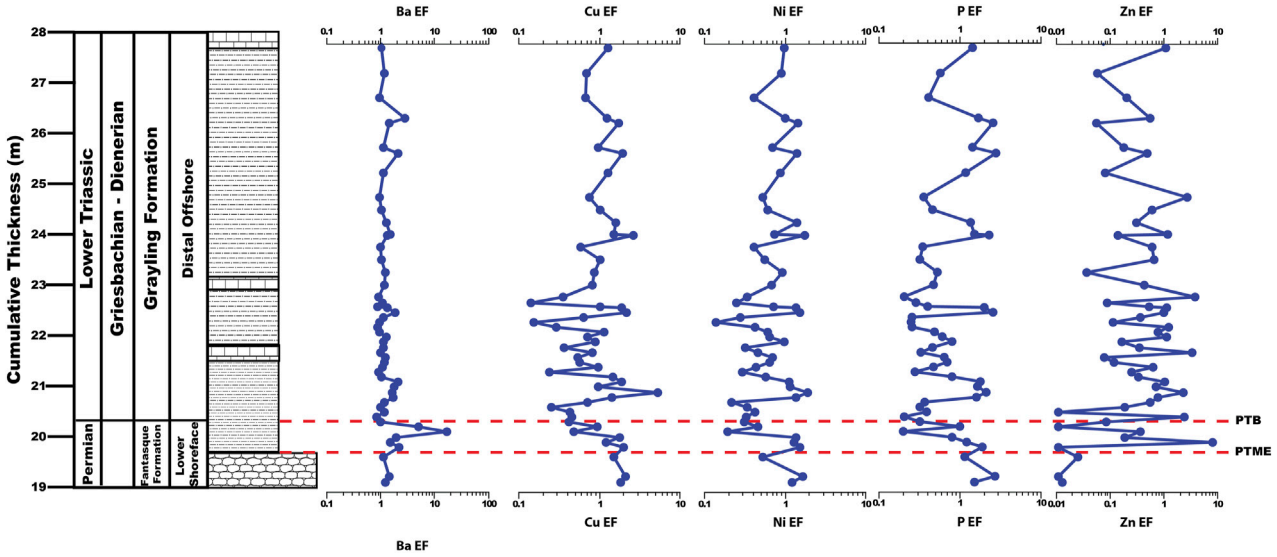

FIGURE 8
Barium, Cu, Ni, P, and Zn enrichment factors (EFs) across the PTB interval, Ursula Creek, BC Canada locality.

Phosphorite deposits in the modern ocean are associated with upwelling zones and areas of high primary productivity, such as off the coast of Peru and Chile (e.g., Burnett, 1977; Burnett et al., 1983); this observation led to the suggestion that phosphorite deposits in the geologic record are an indication of ancient coastal upwelling and high primary productivity (e.g., Diester-Haass and Schrader, 1979; Parrish, 1982; Kametaka et al., 2005). Therefore, the occurrence of phosphate nodules within the Toad Formation, when combined with elevated Ba, Cu, Ni, P, and Zn EFs points to the re-establishment of mid-latitude coastal upwelling and high primary productivity as the planet cooled and shifted away from hothouse conditions (Kidder and Worsley, 2010)

Detrital pyrite layers and lenses found in the Smithian-Spathian portion of the Toad Formation are an unusual feature that has been documented elsewhere in Lower Triassic rocks from the WCSB, and are attributed to euxinic events (Schoepfer et al., 2013). The pyrite layers and lenses at Ursula Creek are closely associated with turbidites within the Toad Formation, suggesting that the two features may be related to each other, and, indeed, a similar relationship has been demonstrated in modern sediments found offshore of Sumatra (Yang et al., 2022). However, the modern sediments undergo extensive bioturbation, which redistributes organic matter, iron (oxy)(hydr) oxides, and SO_4^{2-}, allowing greigite (a precursor to pyrite) to form (Yang et al., 2022). Turbidites found within the Toad Formation are undisturbed by bioturbation, but the presence of bottom water or pore water euxinia may have served as an alternate means to introduce sulphur, while aeolian dust from the arid interior provided a source of iron (Davies, 1997; Jickells et al., 2005; Zonneveld and Moslow, 2014; Zonneveld and Moslow, 2018).

Depositional model

The uppermost Fantasque Formation, Grayling Formation and lower Toad Formation at Ursula Creek provide a continuous record of the PTME and subsequent recovery interval. Upwelling led to the deposition of the chert of the Fantasque Formation (Beauchamp and Baud, 2002), but the deterioration of environmental conditions due to global warming in the Late Permian resulted in the establishment of periodic anoxic conditions in deeper-water settings (Figure 9A) (Beauchamp and Baud, 2002; Wignall and Twitchett, 2002; Wignall and Newton, 2003). The eruption of the Siberian Traps injected enormous volumes of CO_2 into the atmosphere and pushed the planet into a hothouse mode that extended across much of the Early Triassic (Figure 9B) (Sun et al., 2012; Romano et al., 2013). Warm global temperatures near the PTME resulted in a global shift from polar-driven thermohaline circulation to the sinking of warm, salty waters from the mid-latitudes (Kidder and Worsley, 2010). Sluggish bottom-water circulation allowed euxinic conditions to develop in the deep ocean that periodically impinged into shallow settings during transgressions (Kidder and Worsley, 2010), and are recorded by a reduction in pyrite framboid sizes near the base of the Grayling Formation at Ursula Creek (Wignall and Newton, 2003), and by the presence of detrital pyrite layers elsewhere within the WCSB (Schoepfer et al., 2013). Sulfidic deep waters sequestered redox-sensitive trace elements and led to the depletion of Mo, U, and V globally (Algeo, 2004; Xiang et al., 2020; Takahashi et al., 2021), including Mo and V in the lower 20 m of the Grayling Formation. Meanwhile, the rise in productivity across the PTME, represented by a rapid, but short-lived increase in Ba, Cu, Ni, P, and Zn EFs that correlates with the ephemeral productivity increase noted by Schoepfer et al. (2013), and was due to the input of nutrients via runoff immediately following the extinction event (Sephton et al., 2005; Algeo and Twitchett, 2010; Algeo et al., 2011). Productivity otherwise remained low across the lower 6 m of the Grayling Formation (Figure 9C); a similar collapse was also noted at the Opal Creek section by Schoepfer et al. (2012), Schoepfer et al. (2013). Persistently low productivity in the WCSB was the result of high global temperatures that led to the reduction of global temperature gradients, which reduced windspeeds and dampened coastal

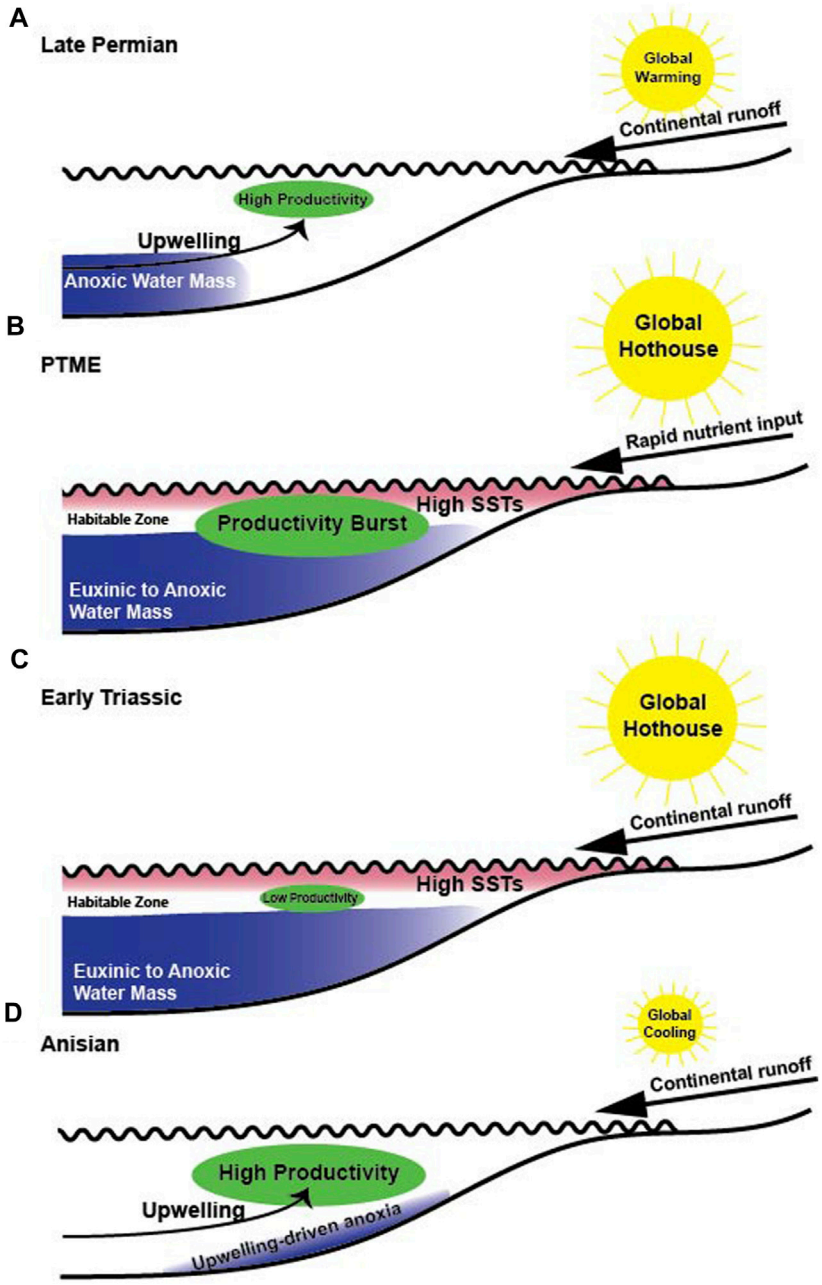

FIGURE 9
Depositional model for the Late Permian-Middle Triassic at Ursula Creek. **(A)** During the Late Permian, upwelling led to the deposition of chert of the Fantasque Formation, but deteriorating environmental conditions due to global warming resulted in the periodic incursion of anoxic waters and the deposition of black shale horizons (Beauchamp and Baud, 2002; Wignall and Newton, 2003; Kiehl and Shields, 2005). **(B)** Eruption of the Siberian Traps led to extreme hothouse conditions as vast amounts of CO_2 were emitted to the atmosphere (e.g., Renne et al., 1995; Wignall, 2001; Rampino et al., 2017; Green et al., 2022). Global hothouse conditions resulted in the development of euxinic bottom waters (Kidder and Worsley, 2010), while rapid nutrient input from the continent led to a productivity rise across the PTME event horizon (Schoepfer et al., 2013). **(C)** Productivity remained low across the Early Triassic, with brief increases in productivity due to runoff, perhaps associated with large storms. **(D)** Decreasing temperatures around the Spathian-Anisian boundary (Sun et al., 2012) led to invigorated upwelling and high productivity that resulted in eutrophication-driven anoxia.

upwelling (Kidder and Worsley, 2010). Cu, Ni, P, and Zn EFs increase across the remainder of the Grayling Formation and the Smithian-Spathian portion of the Toad Formation, indicating that while productivity was dampened during the Early Triassic, it slowly improved over time. The source of nutrients to the WCSB during this time may have been runoff derived from progressively stronger hothouse storms as global temperatures warmed to their highest levels in the late Smithian (Sun et al., 2012), or may be due to a shallowing nutricline (Grasby et al., 2016). Bottom water conditions remained anoxic during the same period, as indicated by the continued lack of benthic fauna and tracemakers, as well as elevated Mo, U, and V EFs. Hothouse conditions ended around

the Spathian-Anisian boundary (Sun et al., 2012), and upwelling was re-established (Figure 9D), as indicated by the presence of phosphate nodules in the upper Toad Formation, as well as sustained high EFs for Cu, Ni, P, and Zn. High productivity, driven by reinvigorated upwelling, was the likely driver of benthic anoxia during deposition of the Anisian portion of the Toad Formation, while the presence of dense *Asteriacites* trace fossils on a limestone bed near the base of the Anisian portion of the unit suggests that palaeoxygenation was more variable, with periods of dysoxic conditions (Savrda et al., 1984).

This study provides the first continuous geochemical record of the PTME and Lower Triassic environmental instability from the western margin of Pangaea. While the Ursula Creek section lacks benthic fauna or trace fossils to compare environmental conditions to recovery trends, it does provide evidence that harsh environmental conditions, specifically anoxic to euxinic deep waters, persisted in offshore settings across the entire extinction and recovery interval, and may have had a dampening effect on biotic recovery. High sea surface temperatures across the same interval would have narrowed the habitable zone (Beatty et al., 2008; Song et al., 2014) and is predicted to have led to a piecemeal recovery that may have experienced multiple stops and starts as environmental conditions shifted (Pietsch et al., 2016; Woods et al., 2019). Indeed, rare *Claraia* impressions have been noted on bedding planes deposited in offshore settings from the upper Griesbachian, as well as in a few horizons from the Dienerian and Smithian (Zonneveld, pers. obs. of core 16-73-83-25W6) suggesting that oxygenation in other parts of the basin was more variable and occasionally dysoxic.

Hyperthermals drive mass extinctions by increasing SSTs and driving deoxygenation of the oceans (Kidder and Worsley, 2010). In the case of the Permian-Triassic mass extinction and its aftermath, the hyperthermal stretched across much of the Early Triassic before atmospheric and oceanic conditions ameliorated in the Middle Triassic (Sun et al., 2012). The Permian-Triassic mass extinction and recovery interval points to the temporal persistence of hyperthermals and associated environmental stresses, and the urgency of curbing modern greenhouse gas emissions before the Earth tips into an anthropogenically-driven hothouse state.

Conclusion

The results of this study offer the following conclusions:

1. Anoxic conditions persisted across the entire study interval, from the upper Fantasque Formation, across the Griesbachian-Dienerian Grayling Formation, and through the Smithian-Spathian portion of the Toad Formation. Most of the Anisian succession was similarly anoxic, with dysoxic conditions in one horizon permitting temporary colonization by epifaunal ophiuroids. Anoxic conditions during the Early Triassic were driven by global hothouse conditions, which led to the production of warm, saline bottom waters and sluggish ocean circulation. Anisian anoxia was likely due to the return of wind-driven upwelling and high coastal productivity as global temperatures decreased.
2. Productivity rose across PTME, perhaps as the result of a brief period of nutrient input following the extinction. Productivity was low during the earliest Triassic (EFs typically <1 from 19.6 to 25.6 m), but began a slow, steady increase across the remainder of the study interval. The formation of phosphate nodules in the Anisian portion of the Toad Formation indicates a return to more typical upwelling behaviour along the western margin of the supercontinent at the beginning of the Middle Triassic.
3. Anoxic to euxinic conditions were present offshore of the WCSB for the entire recovery interval and provided a stress from below, that, when coupled with high SSTs from above, squeezed habitable zones and controlled the timing and shape of biotic recovery from the PTME.
4. Hyperthermals are long-lived and associated with a variety of environmental stresses that can cause mass extinctions and delay the subsequent biotic recovery. Study of past hyperthermals reveal that it is imperative to curb modern greenhouse gas emissions before the planet enters a modern hothouse state.

Data availability statement

The raw data supporting the conclusion of this article will be made available by the authors, without undue reservation.

Author contributions

AW: Conceptualization, Data curation, Formal Analysis, Funding acquisition, Investigation, Methodology, Resources, Writing–original draft. J-PZ: Investigation, Writing–review and editing. RW: Formal Analysis, Investigation, Writing–original draft.

Funding

The author(s) declare financial support was received for the research, authorship, and/or publication of this article. Funding was provided to AW by Petroleum Research Fund grant #47346-B2.

Conflict of interest

The authors declare that the research was conducted in the absence of any commercial or financial relationships that could be construed as a potential conflict of interest.

Publisher's note

References

Algeo, T., Kuwahara, K., Sano, H., Bates, S., Lyons, T., Elswick, E., et al. (2011). Spatial variation in sediment fluxes, redox conditions, and productivity in the Permian-Triassic Panthalassic Ocean. *Palaeogeogr. Palaeoclimatol. Palaeoecol.* 308, 65–83. doi:10.1016/j.palaeo.2010.07.007

Algeo, T. A. (2004). Can marine anoxic events draw down the trace element inventory of seawater? *Geology* 32, 1057–1060. doi:10.1130/g20896.1

Algeo, T. A., Ellwood, B., Nguyen, T. K. T., Rowe, H., and Maynard, J. B. (2007). The Permian–Triassic boundary at Nhi Tao, Vietnam: evidence for recurrent influx of sulfidic watermasses to a shallow-marine carbonate platform. *Palaeogeogr. Palaeoclimatol. Palaeoecol.* 252, 304–327. doi:10.1016/j.palaeo.2006.11.055

Algeo, T. A., and Twitchett, R. J. (2010). Anomalous Early Triassic sediment fluxes due to elevated weathering rates and their biological consequences. *Geology* 38, 1023–1026. doi:10.1130/g31203.1

Alroy, J., Aberhan, M., Bottjer, D. J., Foote, M., Fursich, F. T., Harries, P. J., et al. (2008). Phanerozoic trends in the global diversity of marine invertebrates. *Science* 321, 97–100. doi:10.1126/science.1156963

Baucon, A., and De Carvalho, C. N. (2016). Stars of the aftermath: Asteriacites beds from the lower triassic of the carnic alps (werfen formation, sauris di sopra), Italy. *Palaios* 31, 161–176. doi:10.2110/palo.2015.015

Beatty, T. W., Zonneveld, J.-P., and Henderson, C. (2008). Anomalously diverse Early Triassic ichnofossil assemblages in northwest Pangea: a case for a shallow-marine habitable zone. *Geology* 36, 771–774. doi:10.1130/g24952a.1

Beauchamp, B., and Baud, A. (2002). Growth and demise of Permian biogenic chert along northwest Pangea: evidence for end-Permian collapse of thermohaline circulation. *Palaeogeogr. Palaeoclimatol. Palaeoecol.* 184, 37–63. doi:10.1016/s0031-0182(02)00245-6

Black, B. A., Lamarque, J.-F., Shields, C., Elkins-Tanton, L. T., and Kiehl, J. T. (2015). "Environmental effects of large igneous province magmatism: a Siberian perspective," in *Volcanism and global environmental change*. Editors A. Schmidt, K. E. Fristad, and L. T. Elkins-Tanton (Cambridge: Cambridge University Press), 307–320.

Bond, D. P. G., and Wignall, P. B. (2010). Pyrite framboid study of marine Permian-Triassic boundary sections: a complex anoxic event and its relationship to contemporaneous mass extinction. *Geol. Soc. Am. Bull.* 122, 1265–1279. doi:10.1130/b30042.1

Boyer, D. L., Bottjer, D. J., and Droser, M. L. (2004). Ecological signature of lower triassic shell beds of the western United States. *PALAIOS* 19, 372–380. doi:10.1669/0883-1351(2004)019<0372:esolts>2.0.co;2

Brookfield, M. E., Shellnutt, J. G., Qi, L., Hannigan, R., Bhat, G. M., and Wignall, P. B. (2010). Platinum element group variations at the Permo–Triassic boundary in Kashmir and British Columbia and their significance. *Chem. Geol.* 272, 12–19. doi:10.1016/j.chemgeo.2010.01.008

Brookfield, M. E., Stebbins, A. G., Williams, J. C., and Hannigan, R. E. (2022). Palaeoenvironments and elemental geochemistry across the Permian–Triassic boundary at Ursula Creek, British Columbia, Canada, and a comparison with some other deep-water Permian–Triassic boundary shelf/slope sections in western North America *the Depositional Record. Depos. Rec.* 8, 895–930. doi:10.1002/dep2.187

Burgess, S. D., Muirhead, J. D., and Bowring, S. A. (2017). Initial pulse of Siberian Traps sills as the trigger of the end-Permian mass extinction. *Nat. Commun.* 8, 164. doi:10.1038/s41467-017-00083-9

Burnett, W. C. (1977). Geochemistry and origin of phosphorite deposits from off Peru and Chile. *Geol. Soc. Am. Bull.* 88, 813–823. doi:10.1130/0016-7606(1977)88<813:gaoopd>2.0.co;2

Davies, G. R. (1997a). Aeolian sedimentation and bypass, triassic of western Canada. *Bull. Can. Petroleum Geol.* 45, 624–642.

Davies, G. R. (1997b). The Triassic of the Western Canada sedimentary basin; tectonic and stratigraphic framework, paleogeography, paleoclimate and biota. *Bull. Can. Petroleum Geol.* 45, 434–460.

Davies, G. R., Moslow, T. F., and Sherwin, M. D. (1997). The lower triassic montney formation, west-central Alberta. *Bull. Can. Petroleum Geol.* 45, 474–505.

Dean, W. E., Jr. (1974). Determination of carbonate and organic matter in calcareous sediments and sedimentary rocks by loss on ignition; comparison with other methods. *J. Sediment. Petrology* 44, 242–248. doi:10.1306/74d729d2-2b21-11d7-8648000102c1865d

Diester-Haass, L., and Schrader, H.-J. (1979). Neogene coastal upwelling history off northwest and southwest Africa. *Mar. Geol.* 29, 39–53. doi:10.1016/0025-3227(79)90101-4

Droser, M. L., and Bottjer, D. J. (1986). A semiquantitative field classification of ichnofabric. *J. Sediment. Petrology* 56, 558–559. doi:10.1306/212f89c2-2b24-11d7-8648000102c1865d

Erwin, D. H. (1993). *The great paleozoic crisis; life and death in the permian*. New York: Columbia University Press.

Fan, J. X., Shen, S. Z., Erwin, D. H., Sadler, P. M., Macleod, N., Cheng, Q. M., et al. (2020). A high-resolution summary of Cambrian to Early Triassic marine invertebrate biodiversity. *Science* 367, 272–277. doi:10.1126/science.aax4953

Ferri, F., and Zonneveld, J.-P. (2008). Were triassic rocks of the western Canada Sedimentary Basin deposited in a foreland? *Can. Soc. Petroleum Geol. Reserv.* 35, 12–14.

Galfetti, T., Bucher, H., Martini, R., Hochuli, P. A., Weissert, H., Crasquin-Soleau, S., et al. (2008). Evolution of Early Triassic outer platform paleoenvironments in the Nanpanjiang Basin (South China) and their significance for the biotic recovery. *Sediment. Geol.* 204, 36–60. doi:10.1016/j.sedgeo.2007.12.008

Gibson, D. W., and Edwards, D. E. (1990). *Triassic stratigraphy of the Williston Lake area, northeastern British Columbia*. Calgary: Canadian Society of Petroleum Geologists Field Trip Guidebook, Basin Perspectives.

Gibson, D. W., and Edwards, D. E. (1992). *Triassic stratigraphy and sedimentary environments of the Williston Lake area and adjacent subsurface plains, northeastern British Columbia*. United States: American Association of Petroleum Geologists Annual Convention Field Trip Guide No. 2.

Golding, M. L. (2021). Abundant conodont faunas from the olenekian (early triassic) of subsurface British Columbia, Canada and diversification of the neogondolellinae around the smithian-spathian boundary. *Glob. Planet. Change* 205, 103613. doi:10.1016/j.gloplacha.2021.103613

Grasby, S., and Beauchamp, B. (2009). Latest permian to early triassic basin-to-shelf anoxia in the sverdrup basin, arctic Canada. *Chem. Geol.* 264, 232–246. doi:10.1016/j.chemgeo.2009.03.009

Grasby, S. E., Beauchamp, B., Embry, A., and Sanei, H. (2013). Recurrent early triassic ocean anoxia. *Geology* 41, 175–178. doi:10.1130/g33599.1

Grasby, S. E., Beauchamp, B., and Knies, J. (2016). Early Triassic productivity crises delayed recovery from world's worst mass extinction. *Geology* 44, 779–782. doi:10.1130/g38141.1

Grasby, S. E., Bond, D. P. G., Wignall, P. B., Yin, R., Strachan, L. J., and Takahashi, S. (2021). Transient Permian-Triassic euxinia in the southern Panthalassa deep ocean. *Geology* 49, 889–893. doi:10.1130/g48928.1

Green, T., Renne, P. R., and Keller, C. B. (2022). Continental flood basalts drive Phanerozoic extinctions. *Proc. Natl. Acad. Sci. U. S. A.* 119, e2120441119. doi:10.1073/pnas.2120441119

Hallam, A. (1991). Why was there a delayed radiation after the end-Paleozoic extinctions? *Hist. Biol.* 5, 257–262. doi:10.1080/10292389109380405

Henderson, C. M. (1997). Uppermost Permian conodonts and the Permian-Triassic boundary in the Western Canada sedimentary basin. *Bull. Can. Petroleum Geol.* 45, 693–707.

Henderson, C. M., Golding, M. L., and Orchard, M. J. (2018). Conodont sequence biostratigraphy of the lower triassic montney formation. *Bull. Can. Petroleum Geol.* 66, 7–22.

Henderson, C. M., and Mei, S. (2000). Preliminary cool water permian conodont zonation in north pangea: a review. *Permophiles* 36, 16–23.

Ishizaki, Y., and Shiino, Y. (2023). Sedimentary environment and redox conditions of the lower triassic osawa Formation in the southern kitakami terrane, Japan: insights into ocean redox stratification and faunal recovery. *PALAIOS* 38, 210–232. doi:10.2110/palo.2021.045

Isozaki, Y. (1997). Permo-triassic boundary superanoxia and stratified superocean: records from lost deep sea. *Science* 276, 235–238. doi:10.1126/science.276.5310.235

Jickells, T. D., An, Z. S., Andersen, K. K., Baker, A. R., Bergametti, G., Brooks, N., et al. (2005). Global iron connections between desert dust, ocean biogeochemistry, and climate. *Science* 308, 67–71. doi:10.1126/science.1105959

Joachimski, M. M., Mueller, J., Gallagher, T. M., Mathes, G., Chu, D. L., Mouraviev, F., et al. (2022). Five million years of high atmospheric CO2 in the aftermath of the Permian-Triassic mass extinction. *Geology* 50, 650–654. doi:10.1130/g49714.1

Kametaka, M., Takebe, M., Nagai, H., Zhu, S., and Takayanagi, Y. (2005). Sedimentary environments of the Middle Permian phosphorite-chert complex from the northeastern Yangtze platform, China; the Gufeng Formation: a continental shelf radiolarian chert. *Sediment. Geol.* 174, 197–222. doi:10.1016/j.sedgeo.2004.12.005

Kidder, D. L., and Worsley, T. R. (2004). Causes and consequences of extreme Permo-Triassic warming to globally equable climate and relation to the Permo-Triassic extinction and recovery. *Palaeogeogr. Palaeoclimatol. Palaeoecol.* 203, 207–237. doi:10.1016/s0031-0182(03)00667-9

Kidder, D. L., and Worsley, T. R. (2010). Phanerozoic large igneous provinces (LIPs), HEATT (haline euxinic acidic thermal transgression) episodes, and mass extinctions *palaeogeography, palaeoclimatology, palaeoecology. Palaeogeogr. Palaeoclimatol. Palaeoecol.* 295, 162–191. doi:10.1016/j.palaeo.2010.05.036

Kiehl, J. T., and Shields, C. A. (2005). Climate simulation of the latest Permian: implications for mass extinction. *Geology* 33, 757–760. doi:10.1130/g21654.1

Lau, K. V., Maher, K., Altiner, D., Kelley, B. M., Kump, L. R., Lehrmann, D. J., et al. (2016). Marine anoxia and delayed Earth system recovery after the end-Permian extinction. *Proc. Natl. Acad. Sci. U. S. A.* 113, 2360–2365. doi:10.1073/pnas.1515080113

Lehrmann, D., Payne, J., Felix, S., Dillett, P., Wang, H., Yu, Y., et al. (2003). Permian-Triassic boundary sections from shallow-marine carbonate platforms of the Nanpanjiang Basin, south China: implications for oceanic conditions associated with the end-Permian extinction and its aftermath. *Palaios* 18, 138–152. doi:10.1669/0883-1351(2003)18<138:pbsfsc>2.0.co;2

Liao, W., Wang, Y., Kershaw, S., Weng, Z., and Yang, H. (2010). Shallow-marine dysoxia across the Permian-Triassic boundary: evidence from pyrite framboids in the microbialite in south China. *Sediment. Geol.* 232, 77–83. doi:10.1016/j.sedgeo.2010.09.019

Metcalfe, I., Nicoll, R. S., Willink, R., Ladjavadi, M., and Grice, K. (2013). Early Triassic (Induan–Olenekian) conodont biostratigraphy, global anoxia, carbon isotope excursions and environmental perturbations: new data from Western Australian Gondwana. *Gondwana Res.* 23, 1136–1150. doi:10.1016/j.gr.2012.07.002

Nützel, A., and Schulbert, C. (2005). Facies of two important Early Triassic gastropod lagerstätten: implications for diversity patterns in the aftermath of the end-Permian mass extinction. *Facies* 51, 480–500. doi:10.1007/s10347-005-0074-5

Orchard, M. J., and Tozer, E. T. (1997). Triassic conodont biochronology, its calibration with the ammonoid standard, and a biostratigraphic summary for the Western Canada Sedimentary Basin. *Bull. Can. Petroleum Geol.* 45, 675–692.

Orchard, M. J., and Zonneveld, J.-P. (2009). The lower triassic sulphur mountain Formation in the wapiti Lake area: lithostratigraphy, conodont biostratigraphy, and a new biozonation for the lower olenekian (Smithian)Earth science sector (ESS) contribution 20080714. *Can. J. Earth Sci.* 46, 757–790. doi:10.1139/e09-051

Parrish, J. T. (1982). Upwelling and petroleum source beds, with reference to the Paleozoic. *Am. Assosciation Petroleum Geol. Bull.* 66, 750–774.

Pietsch, C., Mata, S. A., and Bottjer, D. J. (2014). High temperature and low oxygen perturbations drive contrasting benthic recovery dynamics following the end-Permian mass extinction. *Palaeogeogr. Palaeoclimatol. Palaeoecol.* 399, 98–113. doi:10.1016/j.palaeo.2014.02.011

Pietsch, C., Petsios, E., and Bottjer, D. J. (2016). Sudden and extreme hyperthermals, low-oxygen, and sediment influx drove community phase shifts following the end-Permian mass extinction. *Palaeogeogr. Palaeoclimatol. Palaeoecol.* 451, 183–196. doi:10.1016/j.palaeo.2016.02.056

Playter, T., Corlett, H., Konhauser, K. O., Robbins, L., Rohais, S., Crombez, V., et al. (2017). Clinoform identification and correlation in fine-grained sediments: a case study using the Triassic Montney Formation. *Sedimentology* 65, 263–302. doi:10.1111/sed.12403

Proverbs, P., Bann, K. L., Fratton, C. M., Frostad, C. J., and Juska, A. (2018). Facies architecture and sequence stratigraphy of the Lower Triassic Montney Formation, NE British Columbia: fundamental controls on the distribution of 'sweet spots' in a world-class unconventional reservoir. *Bull. Can. Petroleum Geol.* 66, 237–258.

Pruss, S., and Bottjer, D. J. (2004). Early Triassic trace fossils of the western United States and their implications for prolonged environmental stress from the End-Permian mass extinction. *PALAIOS* 19, 551–564. doi:10.1669/0883-1351(2004)019<0551:ettfot>2.0.co;2

Rampino, M. R., Rodriguez, S., Baransky, E., and Cai, Y. (2017). Global nickel anomaly links Siberian Traps eruptions and the latest Permian mass extinction. *Sci. Rep.* 7, 12416. doi:10.1038/s41598-017-12759-9

Raup, D. M. (1979). Size of the Permo-Triassic bottleneck and its evolutionary implications. *Science* 206, 217–218. doi:10.1126/science.206.4415.217

Renne, P. R., Zichao, Z., Richards, M. A., Black, M. T., and Basu, A. R. (1995). Synchrony and causal relations between Permian-Triassic boundary crises and Siberian flood volcanism. *Science* 269, 1413–1416. doi:10.1126/science.269.5229.1413

Richoz, S., Krystyn, L., Baud, A., Brandner, R., Horacek, M., and Mohtat-Aghai, P. (2010). Permian–Triassic boundary interval in the Middle East (Iran and N. Oman): progressive environmental change from detailed carbonate carbon isotope marine curve and sedimentary evolution. *J. Asian Earth Sci.* 39, 236–253. doi:10.1016/j.jseaes.2009.12.014

Riquier, L., Tribovillard, N., Averbuch, O., Joachimski, M. M., Racki, G., Devleeschouwer, X., et al. (2005). "Productivity and bottom water redox conditions at the Frasnian-Fammenian boundary on both sides of the Eovariscan Belt: constraints from trace-element geochemistry," in *Understanding late devonian and permian-triassic biotic and climatic events*. Editors D. J. Over, J. R. Morrow, and P. B. Wignall (Amsterdam: Elsevier), 199–224.

Rohais, S., Crombez, V., Euzen, T., and Zonneveld, J.-P. (2018). Subsidence dynamics of the montney formation (early triassic, western Canada Sedimentary Basin): insights for its geodynamic setting and wider implications. *Bull. Can. Petroleum Geol.* 66, 128–160.

Romano, C., Goudemand, N., Vennemann, T. W., Ware, D., Schneebeli-Hermann, E., Hochuli, P., et al. (2013). Climatic and biotic upheavals following the end-Permian mass extinction. *Nat. Geosci.* 6, 57–60. doi:10.1038/ngeo1667

Sahney, S., and Benton, M. J. (2008). Recovery from the most profound mass extinction of all time. *Proc. R. Soc. B* 275, 759–765. doi:10.1098/rspb.2007.1370

Saito, R., Kaiho, K., Tian, L., and Takahashi, S. (2023). Frequent high-temperature volcanic combustion events delayed biotic recovery after the end-Permian mass extinction. *Earth Planet. Sci. Lett.* 614, 118194. doi:10.1016/j.epsl.2023.118194

Savrda, C. E., Bottjer, D. J., and Gorsline, D. S. (1984). Development of a comprehensive, oxygen-deficient marine biofacies model: evidence from santa monica, san pedro and santa barbara basins, California continetal borderlands. *Am. Assoc. Petroleum Geol. Bull.* 68, 117–1192.

Schoepfer, S. D., Henderson, C. M., Garrison, G. H., Foriel, J., Ward, P. D., Selby, D., et al. (2013). Termination of a continent-margin upwelling system at the permian–triassic boundary (opal Creek, Alberta, Canada). *Glob. Planet. Change* 105, 21–35. doi:10.1016/j.gloplacha.2012.07.005

Schoepfer, S. D., Henderson, C. M., Garrison, G. H., and Ward, P. D. (2012). Cessation of a productive coastal upwelling system in the Panthalassic Ocean at the permian–triassic boundary. *Palaeogeogr. Palaeoclimatol. Palaeoecol.* 313-314, 181–188. doi:10.1016/j.palaeo.2011.10.019

Schubert, J. K. (1989). *Paleoecology of the lower triassic virgin member (moenkopi formation), southeastern Nevada and southwestern Utah*. California: M. S., University of Southern California.

Scotese, C. R. (2021). An atlas of phanerozoic paleogeographic maps: the seas come in and the seas go out. *Annu. Rev. Earth Planet. Sci.* 49, 679–728. doi:10.1146/annurev-earth-081320-064052

Sephton, M., Looy, C., Brinkhuis, H., Wignall, P., De Leeuw, J., and Visscher, H. (2005). Catastrophic soil erosion during the end-Permian biotic crisis. *Geology* 33, 941–944. doi:10.1130/g21784.1

Shen, J., Schoepfer, S. D., Feng, Q. L., Zhou, L., Yu, J. X., Song, H. Y., et al. (2015). Marine productivity changes during the end-Permian crisis and Early Triassic recovery. *Earth-Science Rev.* 149, 136–162. doi:10.1016/j.earscirev.2014.11.002

Sobolev, A. V., Arndt, N. T., Krivolutskaya, A., Kuzmin, D. V., and Sobolev, S. V. (2015). "The origin of gases that caused the Permian-Triassic extinction," in *Volcanism and global environmental change*. Editors A. Schmidt, K. E. Fristad, and L. T. Elkins-Tanton (Cambridge: Cambridge University Press), 147–163.

Son, T. H., Koeberl, C., Ngoc, N. L., and Huyen, D. T. (2007). The Permian-Triassic boundary sections in northern Vietnam (Nhi Tao and Lung Cam sections): carbon-isotope excursion and elemental variations indicate major anoxic event. *Palaeoworld* 16, 51–66. doi:10.1016/j.palwor.2007.05.010

Song, H., Wignall, P. B., Chu, D., Tong, J., Sun, Y., Song, H., et al. (2014). Anoxia/high temperature double whammy during the Permian-Triassic marine crisis and its aftermath. *Sci. Rep.* 4, 4132. doi:10.1038/srep04132

Stanley, S. M. (2016). Estimates of the magnitudes of major marine mass extinctions in earth history. *Proc. Natl. Acad. Sci. U. S. A.* 113, E6325–E6334. doi:10.1073/pnas.1613094113

Sun, Y., Joachimski, M. M., Wignall, P. B., Yan, C., Chen, Y., Jiang, H., et al. (2012). Lethally hot temperatures during the Early Triassic greenhouse. *Science* 338, 366–370. doi:10.1126/science.1224126

Takahashi, S., Hori, R. S., Yamakita, S., Aita, Y., Takemura, A., Ikehara, M., et al. (2021). Progressive development of ocean anoxia in the end-Permian pelagic Panthalassa. *Glob. Planet. Change* 207, 103650. doi:10.1016/j.gloplacha.2021.103650

Thomas, B. M., Willink, R. J., Grice, K., Twitchett, R. J., Purcell, R. R., Archbold, N. W., et al. (2004). Unique marine permian–triassic boundary section from western Australia. *Aust. J. Earth Sci.* 51, 423–430. doi:10.1111/j.1400-0952.2004.01066.x

Tian, X., and Buck, W. R. (2022). Intrusions induce global warming before continental flood basalt volcanism. *Nat. Geosci.* 15, 417–422. doi:10.1038/s41561-022-00939-w

Tozer, E. T. (1994). Canadian Triassic ammonoid faunas. *Geol. Surv. Can. Bull.* 467, 1–663.

Tribovillard, N., Algeo, T. A., Lyons, T. W., and Riboulleau, A. (2006). Trace metals as paleoredox and paleoproductivity proxies: an update. *Chem. Geol.* 232, 12–32. doi:10.1016/j.chemgeo.2006.02.012

Twitchett, R. J., and Barras, C. G. (2004). "Trace fossils in the aftermath of mass extinction events," in *The application of ichnology to palaeoenvironmental and stratigraphic analysis*. Editor D. Mcilroy (London: Geological Society, London Special Publication), 228, 397–418.

Twitchett, R. J., and Wignall, P. B. (1996). Trace fossils and the aftermath of the Permo-Triassic mass extinction: evidence from northern Italy. *Palaeogeogr. Palaeoclimatol. Palaeoecol.* 124, 137–151. doi:10.1016/0031-0182(96)00008-9

Van Der Weijden, C. H. (2002). Pitfalls of normalization of marine geochemical data using a common divisor. *Mar. Geol.* 184, 167–187. doi:10.1016/s0025-3227(01)00297-3

Varol, B., Kos!Un, E., Ünal Pinar, N., and Ayranci, K. (2011). Pyritized mudstone and associated facies in the Permian–Triassic boundaryof the Çürük Dag section, Southern Turkey. *J. Asian Earth Sci.* 40, 1068–1078. doi:10.1016/j.jseaes.2010.11.017

Wang, F. Y., Chen, J., Dai, X., and Song, H. J. (2022). A new Early Triassic brachiopod fauna from southern Tibet, China: implications on brachiopod recovery and the late Smithian extinction in southern Tethys. *J. Paleontology* 96, 1–32. doi:10.1017/jpa.2021.119

Wang, K., Geldsetzer, H. H. J., and Krouse, H. R. (1994). Permian-triassic extinction: organic δ13C evidence from British Columbia, Canada. *Geology* 22, 580–584. doi:10.1130/0091-7613(1994)022<0580:pteoce>2.3.co;2

Wedepohl, K. H. (1971). "Environmental influences on the chemical composition of shales and clays," in *Physics and chemistry of the Earth*. Editors L. H. Ahrens, F. Press, S. K. Runcorn, and H. C. Urey (Oxford: Pergamon), 305–333.

Wedepohl, K. H. (1991). "The composition of the upper Earth's crust and the natural cycles of selected metals," in *Metals and their compounds in the environment*. Editor E. Merian (New York: VCH), 3–17.

Wignall, P. B. (1994). *Black shales*. Oxford: Oxford University Press.

Wignall, P. B. (2001). Large igneous provinces and mass extinctions. *Earth-Science Rev.* 53, 1–33. doi:10.1016/s0012-8252(00)00037-4

Wignall, P. B., and Hallam, A. (1992). Anoxia as a cause of the Permian/Triassic mass extinction: facies evidence from northern Italy and the western United States. *Palaeogeogr. Palaeoclimatol. Palaeoecol.* 93, 21–46. doi:10.1016/0031-0182(92)90182-5

Wignall, P. B., and Newton, R. N. (2003). Contrasting deep-water records from the upper permian and lower triassic of south tibet and British Columbia: evidence for a diachronous mass extinction. *PALAIOS* 18, 153–167. doi:10.1669/0883-1351(2003)18<153:cdrftu>2.0.co;2

Wignall, P. B., and Twitchett, R. J. (1996). Oceanic anoxia and the end Permian mass extinction. *Science* 272, 1155–1158. doi:10.1126/science.272.5265.1155

Wignall, P. B., and Twitchett, R. J. (2002). "Extent, duration, and nature of the Permian-Triassic superanoxic event," in *Catastrophic events and mass extinctions: impacts and beyond*. Editors C. Koeberl and K. C. Macleod (Boulder, CO: Geological Society of America Special Paper 356), 395–413.

Woods, A. D., Alms, P. A., Monarrez, P. M., and Mata, S. A. (2019). The interaction of recovery and environmental conditions: an analysis of the outer shelf edge of western North America during the early Triassic. *Palaeogeogr. Palaeoclimatol. Palaeoecol.* 513, 52–64. doi:10.1016/j.palaeo.2018.05.014

Xiang, L., Zhang, H., Schoepfer, S. D., Cao, C. Q., Zheng, Q. F., Yuan, D. X., et al. (2020). Oceanic redox evolution around the end-Permian mass extinction at Meishan, South China *Palaeogeography, Palaeoclimatology, Palaeoecology*. *Palaeogeogr. Palaeoclimatol. Palaeoecol.* 544, 109626. doi:10.1016/j.palaeo.2020.109626

Xiao, Y., Wu, K., Tian, L., Benton, M. J., Du, Y., Yang, H., et al. (2018). Framboidal pyrite evidence for persistent low oxygen levels in shallow-marine facies of the Nanpanjiang Basin during the Permian-Triassic transition. *Palaeogeogr. Palaeoclimatol. Palaeoecol.* 511, 243–255. doi:10.1016/j.palaeo.2018.08.012

Yang, T., Dekkers, M. J., Zhao, X., Petronotis, K. E., and Chou, Y.-M. (2022). Greigite formation modulated by turbidites and bioturbation in deep-sea sediments offshore Sumatra. *JGR Solid Earth* 127, e2022JB024734. doi:10.1029/2022jb024734

Zhu, Z. C., Liu, Y. Q., Kuang, H. W., Newell, A. J., Peng, N., Cui, M. M., et al. (2022). Improving paleoenvironment in North China aided Triassic biotic recovery on land following the end-Permian mass extinction. *Glob. Planet. Change* 216, 103914. doi:10.1016/j.gloplacha.2022.103914

Ziegler, C. L., and Murray, R. W. (2007). "Analytical sediment chemistry on board the JOIDES Resolution: a comparison of shipboard and shorebased sample preparation protocols," in *Proceedings of the ocean drilling program, scientific results volume 206*. Editors D. a.H. Teagle, D. S. Wilson, G. D. Acton, and D. A. Vanko (College Station, TX: Ocean Drilling Program), 1–26.

Zonneveld, J.-P. (2010). *The triassic of northeastern British Columbia: sedimentary characteristics & stratigraphic architecture of conventional and unconventional reservoir successions*. Calgary: Canadian Society of Petroleum Geologists CSPG18FT.

Zonneveld, J.-P., Gingras, M. K., and Beatty, T. W. (2010a). Diverse ichnofossil assemblages following the P-T mass extinction, Lower Trissic, Alberta and British Columbia, Canada: evidence for shallow marine refugia on the northwestern coast of Pangaea. *PALAIOS* 25, 368–392. doi:10.2110/palo.2009.p09-135r

Zonneveld, J.-P., Macnaughton, R. B., Utting, J., Beatty, T. W., Pemberton, S. G., and Henderson, C. M. (2010b). Sedimentology and ichnology of the lower triassic montney Formation in the pedigree-ring/border-kahntah river area, northwestern Alberta and northeastern British Columbia. *Bull. Can. Petroleum Geol.* 58, 115–140. doi:10.2113/gscpgbull.58.2.115

Zonneveld, J.-P., and Moslow, T. F. (2014). Perennial river deltas of the montney formation: Alberta and British Columbia subcrop edge. *Geoconvention*.

Zonneveld, J.-P., and Moslow, T. F. (2018). Palaeogeographic setting, lithostratigrahy and sedimentary framework of the lower triassic montney formation of western Alberta and northeastern British Columbia. *Bull. Can. Petroleum Geol.* 66, 93–127.